CHAPTER 4

GEOCHEMISTRY

4.1 Sample Preparation

The rock samples particularly with no sign of carbonate minerals were examined petrographically under the microscope to obtain least-altered samples and to avoid those showing

1) extensive replacement of secondary minerals such as quartz, epidote minerals, albite, carbonates and chlorite;
2) abundant vesicles, amygdales, xenocrysts and xenoliths;
3) well-developed foliation and mineral layering; and
4) abundant veined minerals such as epidote minerals, quartz and calcite and /or patches totally more than approximately 5 modal %

The least-altered 33 samples were selected and done for powder samples to measure for whole-rock chemistry. These powder samples were chemically analyzed for major oxides, trace elements and loss on ignition (herein LOI). The representatives of the least-altered samples were analyzed for rare-earth elements (herein REE).

The analyzed powder samples were carefully prepared by cutting off the weathering surfaces of the least-altered samples, and then splitting into conveniently sized fragments and crushing into small chips (approximately 5 mm across) using Rocklabs Hydraulic Splitter and Jaw Crusher. After that, the rock chips were selected to avoid veins, vesicles, amygdales, xenecrysts, xenoliths and weathering surfaces, and were cleaned to make powder samples. The cleaned rock chips were divided by quartering into 50-80 g and then were pulverized by Rocklabs Tungsten Carbide Ring Mill to be powder samples. The powder samples were prepared at the Department of Geological Sciences, Chiang Mai University, Thailand.

4.2 Analytical Techniques

4.2.1 Major Oxides and Trace Elements Analysis

The chemical analysis of major oxides (SiO_2, TiO_2, Al_2O_3, Fe total as Fe_2O_3, MnO, MgO, CaO, Na_2O, K_2O and P_2O_5) and trace elements (Rb, Sr, Zr, Y, Nb, Ni, Cr, V and Sc) were made up by a Phillip-MagixPro PW 2400 Wavelength Dispersive X-Ray Fluorescence (XRF) Spectrometer, fixed at the Department of Geological Sciences, Chiang Mai University. The instrumental parameters consist of Rhodium tube with a lithium fluoride 200 crystal (used in an elemental range of K-Ru), and scintillation and flow proportion detectors, and X-ray tube operated at 60 kV and current of up to 125 mA; at a maximum powder level of 4 kW. The net (background corrected) intensities were measured, subsequently, calculated against the calibrations derived from 7 international standard reference materials (AGV-2, BCR-2, BHVO-2, BIR-1, DNC-1, GSP-2 and W-2). The inter-elements matrix corrections were done by the Super Q version 3.0 program. The reporting detection limit is about 0.001% for major oxides and 3 ppm for trace elements. The accuracy and precision for most of the elements are better than 5%.

The major oxides analysis was measured from fusion disc samples. Fusion disc was done by mixing 0.8 g powder sample with 0.06 g lithium bromide (LiBr) and 4.0 g di-lithium tetraborate ($Li_2B_4O_7$) in a platinum crucible. The mixture was fused by Burners, and then cools down in a 3 cm platinum mold. The trace element analysis was measured from pressed powder (pellet) by mixing 5.0 g powder sample with 0.3 g wax ($C_6H_8O_3N_2$) in an aluminum cup filled by 3.0 g boric acid (H_3BO_3), and then pressed by a hydraulic machine at 200 kN for 1 minute.

4.2.2 Loss on Ignition Determination

Loss on ignition (LOI) was analyzed by heating a platinum crucible contained 1.0 g sample in a furnace at 1000^{o}C for 12 hours at the Department of Geological Sciences, Chiang Mai University. Powder sample approximately 1.0 g must be weighed before and after heating for calculating LOI.

4.2.3 Rare Earth Element Analysis

The six representative samples were selected for low abundance trace elements (Hf, Th and Ta) and rare earth elements (La, Ce, Pr, Nd, Sm, Eu, Gd, Tb, Dy, Ho, Er, Tm and Yb) analyses using a Perkin-Elmer Scix ELAN 6000 inductively coupled plasma mass spectrometry (ICP-MS) at the Guangzhou Institute of Geochemistry, Chinese Academy of Science, following the methods of Qi *et al*. (2007) and Chen *et al.* (2010). All the samples were grounded and pass through a 75 µm sieve and died at 105 ^{o}C for 4 hours. After drying, a 50 mg of powdered whole-rock sample was digested using added 1.0 ml of analytical reagent grade HF, 3.0 ml of analytical reagent grade HNO_3 and $HClO_3$ in a screw-top Teflon breaker for 2 days at 100 ^{o}C, followed by evaporation to dryness at 140 ^{o}C. Then, the residue was digested in a screw-top PTFE-lined strain-less steel bomb at 190 ^{o}C for 48 hours. After digestion, the solution was evaporated to dryness again to remove Si and residue HF and the residue was dissolved using 4 ml of 50% HNO_3 in a screw-top PTFE-lined strain-less steel bomb at 170 ^{o}C for 4 hours. After cooling, 500 ng Rh was added into the solution as internal solution standard to monitor instrument drift. The final solution reached 50 ml by adding distilled deionized water. In order to protect the ICP-MS, a 1 ml solution of each sample was separated and diluted to 4 ml by addition of 4% HNO_3. For most of the trace elements, analytical precision and accuracy are better than 10%. USGS reference standards (BHVO-2, AGV-2, GSD-9, GSR-1, GSR-2, GSR-3, W-2, SY4, and SARM-4) were chosen as external calibration standards for calculating the element concentrations in the measured samples.

The analytical results for major oxides and trace elements of the studied mafic igneous samples are reported in Table 4.1 and the REE, Ta and Hf analysis of representative samples are given in Table 4.2.

4.3 Element Mobility

The studied mafic igneous rocks have experiences variable degrees of alteration and/or metamorphism. Most commonly, element mobility (Rollison, 1993)

Table 4.1 Whole-rock analyses and some selected ratios of the studied least-altered mafic igneous rocks.

Sample no.	MS16B1*	MS15B2*	MS12B3*	MS14B3*	MS8B4*
Major oxide (wt%)					
SiO_2	51.10	53.54	49.83	61.04	54.57
TiO_2	1.19	1.16	1.13	0.90	1.03
Al_2O_3	15.19	18.16	18.40	18.11	16.28
FeO*	10.04	10.16	11.13	6.09	9.72
MnO	0.12	0.09	0.14	0.08	0.12
MgO	5.80	3.54	5.60	2.50	4.70
CaO	5.89	6.69	8.24	4.54	6.81
Na_2O	3.11	2.57	1.59	3.31	2.17
K_2O	0.26	1.24	1.09	0.95	1.44
P_2O_5	0.20	0.72	0.21	0.24	0.49
LOI	6.89	2.12	2.80	2.40	2.60
Original Sum	99.80	100.00	100.17	100.17	99.93
FeO*/MgO	1.73	2.87	1.99	2.43	2.07
Trace elements (ppm)					
Ba	435.79	643.73	461.72	707.92	964.21
Rb	15.95	33.68	57.97	34.01	59.84
Sr	430.27	629.76	385.40	518.71	428.38
Y	17.02	17.86	17.59	18.75	18.69
Zr	108.39	127.81	68.74	314.74	115.60
Nb	4.52	7.20	4.34	13.13	12.32
Ni	93.12	21.98	35.95	36.10	37.13
Cr	229.11	60.52	130.54	75.88	131.30
V	180.65	186.67	180.02	149.41	169.43
Sc	24.77	26.61	30.89	19.21	22.32
Th	0.39	0.46	0.32	7.73	2.97
Selected elements ratios					
Zr/TiO_2	90.84	109.97	60.82	349.25	112.21
Nb/Y	0.27	0.40	0.25	0.70	0.66
Nb/Zr	0.04	0.06	0.06	0.04	0.11
Y/Zr	0.16	0.14	0.26	0.06	0.16

FeO*=total iron as FeO; LOI=loss on ignition
Oxides other than LOI, and trace elements were analyzed by XRF
*=Group I; **=Group II

Table 4.1 Continued

Sample no.	MS9B4*	MS10B4*	MS6.2B5*	MS6.3B5(B)*	MS6.3B5(D)*
Major oxide (wt%)					
SiO_2	50.93	53.96	54.43	51.86	55.90
TiO_2	1.45	0.43	1.04	1.22	1.23
Al_2O_3	12.92	11.55	15.00	16.25	17.65
FeO*	12.30	9.84	11.12	10.13	8.03
MnO	0.17	0.17	0.17	0.13	0.13
MgO	8.43	10.52	5.38	6.44	3.68
CaO	8.03	7.72	6.69	6.39	5.52
Na_2O	2.01	2.09	2.06	2.68	3.16
K_2O	0.63	0.43	1.74	1.30	1.88
P_2O_5	0.58	0.06	0.19	0.30	0.34
LOI	2.55	2.97	1.84	3.25	2.52
Original Sum	100.00	99.74	99.66	99.96	100.04
FeO*/MgO	1.46	0.94	2.07	1.57	2.19
Trace elements (ppm)					
Ba	425.81	627.46	743.90	657.04	806.57
Rb	21.51	18.66	58.83	51.59	75.33
Sr	263.86	116.41	252.01	352.87	481.67
Y	17.64	17.09	23.87	18.02	19.19
Zr	65.26	55.02	193.43	89.22	300.45
Nb	7.44	1.83	16.72	3.50	13.80
Ni	88.28	209.23	73.30	94.86	40.13
Cr	381.26	1102.10	291.01	223.47	98.37
V	218.81	70.12	171.71	199.69	203.25
Sc	28.68	28.48	26.13	25.45	20.93
Th	10.46	3.08	9.29	9.04	3.47
Selected elements ratios					
Zr/TiO_2	44.91	128.79	186.13	73.00	244.63
Nb/Y	0.42	0.11	0.70	0.19	0.72
Nb/Zr	0.11	0.03	0.09	0.04	0.05
Y/Zr	0.27	0.31	0.12	0.20	0.06

FeO*=total iron as FeO; LOI=loss on ignition

Oxides other than LOI, and trace elements were analyzed by XRF

*=Group I; **=Group II

Table 4.1 Continued

Sample no.	MS65B5*	MS68B5*	MS5B6(13)*	MS5B6(14)*	MC69.1B1**
Major oxide (wt%)					
SiO_2	50.68	51.96	53.82	51.74	47.86
TiO_2	1.37	2.31	1.10	1.38	1.97
Al_2O_3	16.78	13.35	8.83	9.90	16.53
FeO*	11.89	14.95	11.64	13.53	13.09
MnO	0.16	0.14	0.13	0.12	0.16
MgO	4.79	4.93	10.85	9.68	6.78
CaO	8.16	7.79	9.62	9.37	8.13
Na_2O	2.13	2.01	1.01	1.03	2.04
K_2O	1.07	0.52	0.98	0.76	0.43
P_2O_5	0.42	0.41	0.16	0.31	0.45
LOI	2.82	1.53	1.90	1.95	2.81
Original Sum	100.27	99.89	100.02	99.77	100.26
FeO*/MgO	2.48	3.03	1.07	1.40	1.93
Trace elements (ppm)					
Ba	489.80	140.03	471.45	407.55	233.55
Rb	37.06	11.93	31.79	22.95	25.12
Sr	647.54	239.38	107.05	123.26	290.47
Y	17.64	18.51	17.79	18.48	18.32
Zr	103.75	121.77	33.42	68.12	119.49
Nb	6.85	9.27	8.65	11.02	6.99
Ni	22.34	54.23	155.99	101.61	85.52
Cr	54.45	111.89	804.45	614.68	78.28
V	229.12	374.68	172.10	214.81	313.47
Sc	28.93	31.14	33.65	33.89	32.03
Th	7.66	6.77	4.04	10.95	4.01
Selected elements ratios					
Zr/TiO_2	75.50	52.80	30.46	49.46	60.59
Nb/Y	0.39	0.50	0.49	0.60	0.38
Nb/Zr	0.07	0.08	0.26	0.16	0.06
Y/Zr	0.17	0.15	0.53	0.27	0.15

FeO*=total iron as FeO; LOI=loss on ignition

Oxides other than LOI, and trace elements were analyzed by XRF

*=Group I; **=Group II

Table 4.1 Continued

Sample no.	MC17.2B2**	MC18B2**	MC37B3(B)**	MC37B3(D)**	MC39B3**
Major oxide (wt%)					
SiO_2	49.94	47.47	52.22	52.27	44.62
TiO_2	1.44	0.94	0.71	0.19	1.69
Al_2O_3	16.71	19.51	19.79	22.56	16.77
FeO*	14.27	12.59	9.50	4.56	16.74
MnO	0.23	0.11	0.16	0.06	0.18
MgO	6.06	6.85	4.18	4.67	5.05
CaO	9.72	11.74	8.00	9.48	9.87
Na_2O	1.28	0.76	2.95	2.28	1.87
K_2O	0.04	0.02	0.07	0.11	0.06
P_2O_5	0.34	0.01	0.67	0.03	1.86
LOI	0.35	0.09	1.62	3.46	1.17
Original Sum	100.37	100.11	99.88	99.66	99.88
FeO*/MgO	2.35	1.84	2.27	0.98	3.32
Trace elements (ppm)					
Ba	288.82	426.83	584.80	692.27	264.92
Rb	7.37	6.90	6.34	3.00	7.71
Sr	213.63	219.11	867.90	983.11	660.88
Y	16.69	15.78	16.24	15.40	16.27
Zr	16.33	14.73	62.19	74.19	49.39
Nb	4.43	2.28	0.91	0.49	2.49
Ni	29.29	25.48	19.66	31.30	14.32
Cr	104.38	128.76	43.17	54.88	13.89
V	227.02	143.19	99.73	27.74	260.49
Sc	33.47	41.79	29.40	38.03	38.77
Th	8.26	8.26	2.66	2.62	0.71
Selected elements ratios					
Zr/TiO_2	11.36	15.63	87.94	396.31	29.24
Nb/Y	0.27	0.14	0.06	0.03	0.15
Nb/Zr	0.27	0.15	0.01	0.01	0.05
Y/Zr	1.02	1.07	0.26	0.21	0.33

FeO*=total iron as FeO; LOI=loss on ignition

Oxides other than LOI, and trace elements were analyzed by XRF

*=Group I; **=Group II

Table 4.1 Continued

Sample no.	MC40B3**	MC20B4**	MC64B4**	MC64.3B4**	MC25B5**
Major oxide (wt%)					
SiO_2	55.67	47.11	44.22	45.01	46.18
TiO_2	0.89	1.48	1.66	1.69	1.51
Al_2O_3	16.43	20.03	17.99	21.05	19.02
FeO*	10.27	13.41	16.61	13.79	12.77
MnO	0.13	0.12	0.13	0.12	0.21
MgO	4.01	4.95	5.15	4.55	5.00
CaO	7.92	9.54	9.77	9.75	9.57
Na_2O	2.63	1.64	1.47	1.49	1.94
K_2O	0.15	0.26	0.07	0.08	0.02
P_2O_5	0.60	0.05	0.03	0.04	0.38
LOI	1.07	2.15	2.86	2.44	3.60
Original Sum	99.78	100.73	99.96	100.00	100.20
FeO*/MgO	2.56	2.71	3.23	3.03	2.55
Trace elements (ppm)					
Ba	514.29	328.43	246.84	274.73	282.88
Rb	6.28	8.62	9.79	6.89	6.77
Sr	645.81	250.44	214.89	252.28	230.84
Y	16.96	15.94	15.79	15.78	16.86
Zr	87.23	22.76	17.67	20.47	20.09
Nb	3.02	2.23	4.24	3.92	4.30
Ni	28.31	24.16	12.58	28.42	31.28
Cr	35.82	62.18	25.00	70.76	57.63
V	141.14	223.94	265.32	249.96	231.77
Sc	30.74	34.88	39.01	35.83	34.00
Th	7.23	7.55	1.24	7.16	10.00
Selected elements ratios					
Zr/TiO_2	97.55	15.38	10.64	12.15	13.32
Nb/Y	0.18	0.14	0.27	0.25	0.26
Nb/Zr	0.03	0.10	0.24	0.19	0.21
Y/Zr	0.19	0.70	0.89	0.77	0.84

FeO*=total iron as FeO; LOI=loss on ignition

Oxides other than LOI, and trace elements were analyzed by XRF

*=Group I; **=Group II

Table 4.1 Continued

Sample no.	MC44.2B8**	MC45B8**	MC47B8**	MC48B8**	MC53B8**
Major oxide (wt%)					
SiO_2	52.28	52.40	44.34	51.90	51.56
TiO_2	0.57	0.85	1.68	0.61	1.24
Al_2O_3	16.00	17.32	17.95	17.80	16.90
FeO*	9.83	9.53	17.17	8.36	9.54
MnO	0.16	0.13	0.14	0.12	0.11
MgO	6.87	6.48	6.39	7.88	6.28
CaO	12.04	10.75	10.52	11.55	9.10
Na_2O	1.07	1.68	0.86	1.44	2.59
K_2O	0.03	0.08	0.01	0.01	0.13
P_2O_5	0.06	0.11	0.01	0.06	0.19
LOI	0.77	0.83	0.91	0.34	2.52
Original Sum	99.67	100.16	99.97	100.06	100.17
FeO*/MgO	1.43	1.47	2.69	1.06	1.52
Trace elements (ppm)					
Ba	539.53	462.01	214.16	522.10	417.71
Rb	8.01	5.17	5.32	7.87	6.37
Sr	191.70	214.46	176.99	247.21	330.06
Y	16.84	17.08	15.81	16.01	17.65
Zr	21.22	32.22	10.52	23.34	119.38
Nb	2.12	2.84	2.85	3.42	5.71
Ni	50.84	42.75	19.31	63.41	60.29
Cr	141.39	177.96	39.47	254.44	163.34
V	87.81	130.16	272.56	88.61	185.68
Sc	44.30	39.93	38.92	40.00	35.04
Th	2.73	6.84	8.05	3.26	8.79
Selected elements ratios					
Zr/TiO_2	37.35	38.12	6.28	38.57	96.10
Nb/Y	0.13	0.17	0.18	0.21	0.32
Nb/Zr	0.10	0.09	0.27	0.15	0.05
Y/Zr	0.79	0.53	1.50	0.69	0.15

FeO*=total iron as FeO; LOI=loss on ignition

Oxides other than LOI, and trace elements were analyzed by XRF

*=Group I; **=Group II

Table 4.1 Continued

Sample no.	MC56B8**	MC60B8**	MC63B8**
Major oxide (wt%)			
SiO_2	46.02	44.92	46.55
TiO_2	2.12	1.53	1.60
Al_2O_3	18.82	17.24	16.79
FeO*	15.50	16.78	16.67
MnO	0.17	0.16	0.10
MgO	5.28	7.12	6.32
CaO	9.74	10.55	10.14
Na_2O	1.34	0.82	1.36
K_2O	0.02	0.04	0.07
P_2O_5	0.16	0.01	0.02
LOI	0.81	0.84	0.78
Original Sum	100.01	100.03	100.38
FeO*/MgO	2.93	2.36	2.64
Trace elements (ppm)			
Ba	96.93	273.32	299.56
Rb	6.33	7.06	9.16
Sr	214.00	184.89	182.59
Y	15.91	15.51	15.67
Zr	13.82	14.19	12.07
Nb	3.73	3.36	4.16
Ni	13.72	24.41	22.25
Cr	20.61	62.12	76.11
V	337.16	251.61	268.58
Sc	35.52	39.29	36.02
Th	12.27	0.85	2.69
Selected elements ratios			
Zr/TiO_2	6.52	9.25	7.54
Nb/Y	0.23	0.22	0.27
Nb/Zr	0.27	0.24	0.34
Y/Zr	1.15	1.09	1.30

FeO*=total iron as FeO; LOI=loss on ignition

Oxides other than LOI, and trace elements were analyzed by XRF

*=Group I; **=Group II

Table 4.2 REE, Hf and Ta analyses (ppm), and some selected chondrite-normalized ratios of the studied least-altered mafic igneous rocks.

Sample no.	MS14B3*	MS8B4*	MS5B6(13)*	MC37B3(B)**	MC64B4**	MC53B8**
La	33.28	19.81	15.2	7.281	1.096	11.46
Ce	65.58	40.01	40.5	16.06	2.685	25.86
Pr	8.569	5.421	5.983	2.397	0.455	3.608
Nd	33.53	22.96	24.49	11.95	2.375	15.92
Sm	6.634	4.972	5.317	2.668	0.785	3.818
Eu	1.754	1.466	1.391	1.536	0.591	1.324
Gd	6.068	4.942	5.247	2.78	1.127	4.254
Tb	0.987	0.813	0.866	0.4	0.203	0.748
Dy	5.608	4.649	4.94	2.144	1.217	4.53
Ho	1.132	0.985	1.061	0.456	0.28	1.009
Er	3.024	2.694	2.795	1.165	0.709	2.734
Tm	0.414	0.367	0.406	0.153	0.098	0.411
Yb	2.705	2.511	2.7	0.944	0.637	2.635
Hf	6.928	2.626	1.896	0.123	0.276	2.938
Ta	1.067	0.866	1.228	0.084	0.049	0.339
Selected ratio						
[La/Sm]cn	3.060	2.430	1.744	1.665	0.852	1.831
[Sm/Yb]cn	2.649	2.138	2.127	3.052	1.331	1.565

*=Group I; **=Group II
cn=chondrite-normalized values.

will take place during weathering, diagenesis and metamorphism or through interaction with a hydrothermal fluid. Therefore, the chemical compositions of the studied rocks are unlikely to represent the primary compositions derived from magma. The concentrations of some major elements in ancient igneous rocks, such as Si, Ca and alkalis are sensitive to increasing/decreasing during magmatic evolution. However, it is generally agreed that total iron as FeO (herein FeO*) and MgO are slightly removed from primary values. Trace element mobility (Rollison, 1993) is controlled by the mineralogical changes which take place during alteration and nature of fluid phase. The incompatible elements which belong to the LFS group are mobile, whereas the HFS elements (Ti, Zr, Y, Nb, Ta, Th and P) and transitional elements (Ni, Cr, V and Sc) are immobile. The concentrations and the ratios of the immobile

elements remain constant in both unaltered and altered rocks. In addition, Zr is an immobile incompatible elements (Green, 1980) used as a fractionation parameter for the studied rock samples. Also, occasion reports have appeared REE-, especially light REE (LREE), mobility during hydrothermal alteration and low grade metamorphism (Hellman and Henderson, 1979; Whiterford *et al*., 1988), the overwhelming consensus is that the REE patterns of carefully selected samples are probably slightly shifted from their primary patterns, but remain parallel/subparallel to the primary patterns.

These chemical composition ratios, especially immobile incompatible elements; HFSE, transitional elements and REE, have been focused to be used for identification of rocks and determining magma characteristics because they are closely representative of magma. Moreover, the chemical compositions will provide for interpretation of tectonic setting by using discrimination diagram and correlation with modern magma suites.

4.4 Magmatic Affinities of Mafic Igneous Rocks

The representatives of mafic igneous rocks presented in this study show different types of REE patterns, N-MORB normalized multi-element patterns and variation diagram. Using these mutli-element patterns, the studied mafic rocks can be separated into two magmatic groups as Group I (sample number MS16B1, MS15B2, MS12B3, MS14B3 MS8B4, MS9B4, MS10B4, MS6.2B5, MS6.3B5(B), MS6.3B5(D), MS65B5, MS68B5, MS5B6(13) and MS5B6(14)) and Group II (sample number MC69.1B1, MC17.2B2, MC18B2, MC37B3(B), MC37B3(D), MC39B3, MC40B3, MC20B4, MC64B4, MC64.3B4, MC25B5, MC44.2B8, MC45B8, MC47B8, MC48B8, MC53B8, MC56B8, MC60B8 and MC63B8). The Group I rocks were collected from Mae Sai area, and are composed of gabbro, diorite, monzodiorite, microgabbro, microdiorite and andesite/basalt(dike). They have Zr/TiO_2 against Nb/Y ratios in ranges of 0.030-0.0349 and 0.1071-0.7191, respectively, corresponding transitional to subalkalic series (Fig 4.1). The Group II rocks were collected from the Mae Chan area that include mainly gabbro, diorite,

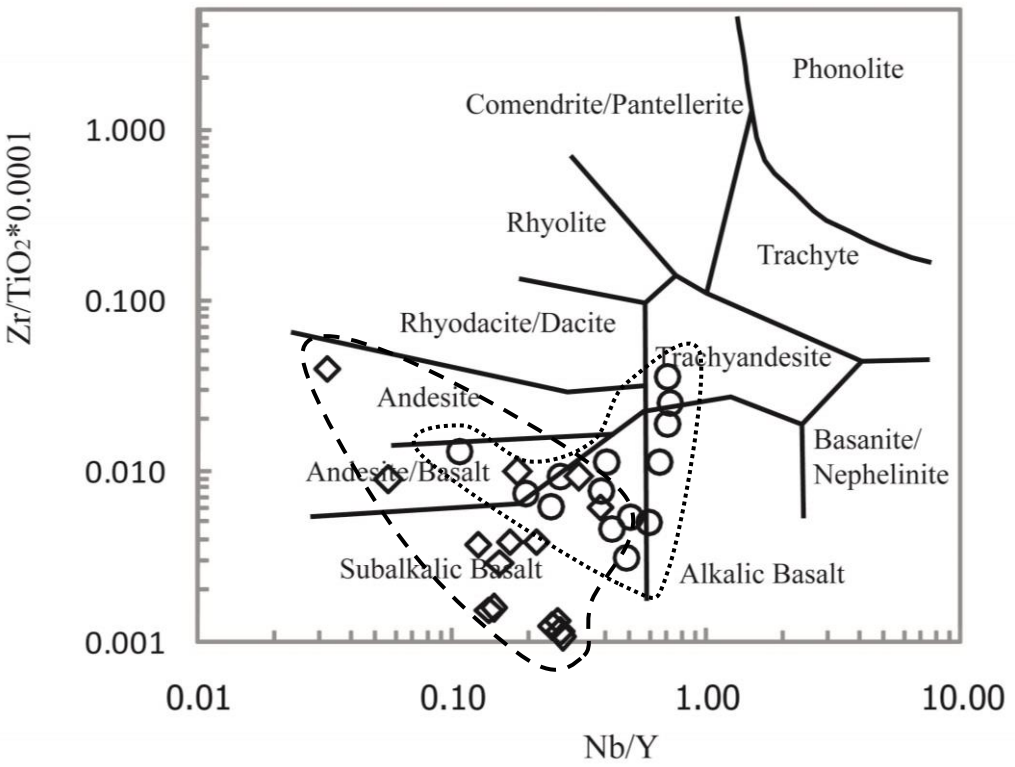

Figure 4.1 Plot of Zr/TiO_2 against Nb/Y for the studied, least-altered mafic igneous rocks (open circle=Group I, and open diamond = Group II). Field boundaries for different magma types are after Winchester and Floyd (1977).

microgabbro, microdiorite/microgabbro, andesite/basalt and basalt. They have Zr/TiO_2 against Nb/Y ratios in ranges of 0.0006-0.0396 and 0.0318-0.3235, respectively. These compositional ranges correspond to subalkalic series (Fig4.1). Three samples of the Group I rocks (sample number MS14B2, MS8B4 and MS5B6(13)) were selected for REE analyses. Three samples of the Group I rocks show a relatively flat REE patterns from Sm to Yb, with chondrite-normalized Sm/Yb [herein (Sm/Yb)cn]=2.127-2.649, and slightly LREE enriched, with chondrite-normalized La/Sm [herein (La/Sm)cn=1.744-3.060] (Fig 4.2a). These REE patterns are typical of tholeiitic series. The Group II rocks (sample number MC37B3(B), MC64B4 and MC53B8) have relatively flat REE pattern from Gd to Yb, with chondrite-normalized Sm/Yb [herein (Sm/Yb)cn]=1.331-3.052, and flat to slightly LREE enrichment, with chondrite-normalized La/Sm [herein (La/Sm)cn=0.852-1.831], correspond to typical of tholeiitic series (Fig 4.2b). The REE patterns for the Group II rocks have positive Eu anomaly, are controlled by cumulative plagioclase. In term of N-MORB normalized multi-element patterns, the Group I rocks general show step-like patterns, characteristics of within-plate basalt (Fig 4.3a). N-MORB normalized multi-element patterns for the Group II rocks they present flat pattern, negative niobium anomalies (Fig 4.3b). Nb anomalies are characteristic of the continental crust and may be an indicator of crustal involvement in magma process (Rollison, 1993).

The variation diagrams for least-mobile elements of the Group I rocks and II rocks, using Zr as a fractionation parameter are shown in Fig 4.4 for major oxides and Fig 4.5 for trace elements. The values of Zr for the Group I rocks are largely higher than those for Group II rocks.

Group I, the diagrams show (1) positive trends for SiO_2, Al_2O_3, K_2O, Sr and Ba, (2) positive trends in the early stage and negative trends in the later stage for TiO_2, Na_2O, P_2O_5, FeO*, MnO, Y, V, Nb and Rb, and (3) Strongly negative trends in the early stage and slightly negative trends in the later stage for CaO, MgO, Ni, Cr, Sr and Sc. These plotting suggest that olivine, chromian spinel, orthopyroxene/ clinopyroxene and/or amphibole fractionate in the early stage and Fe-Ti oxides fractionate in the later stage for derived magma.

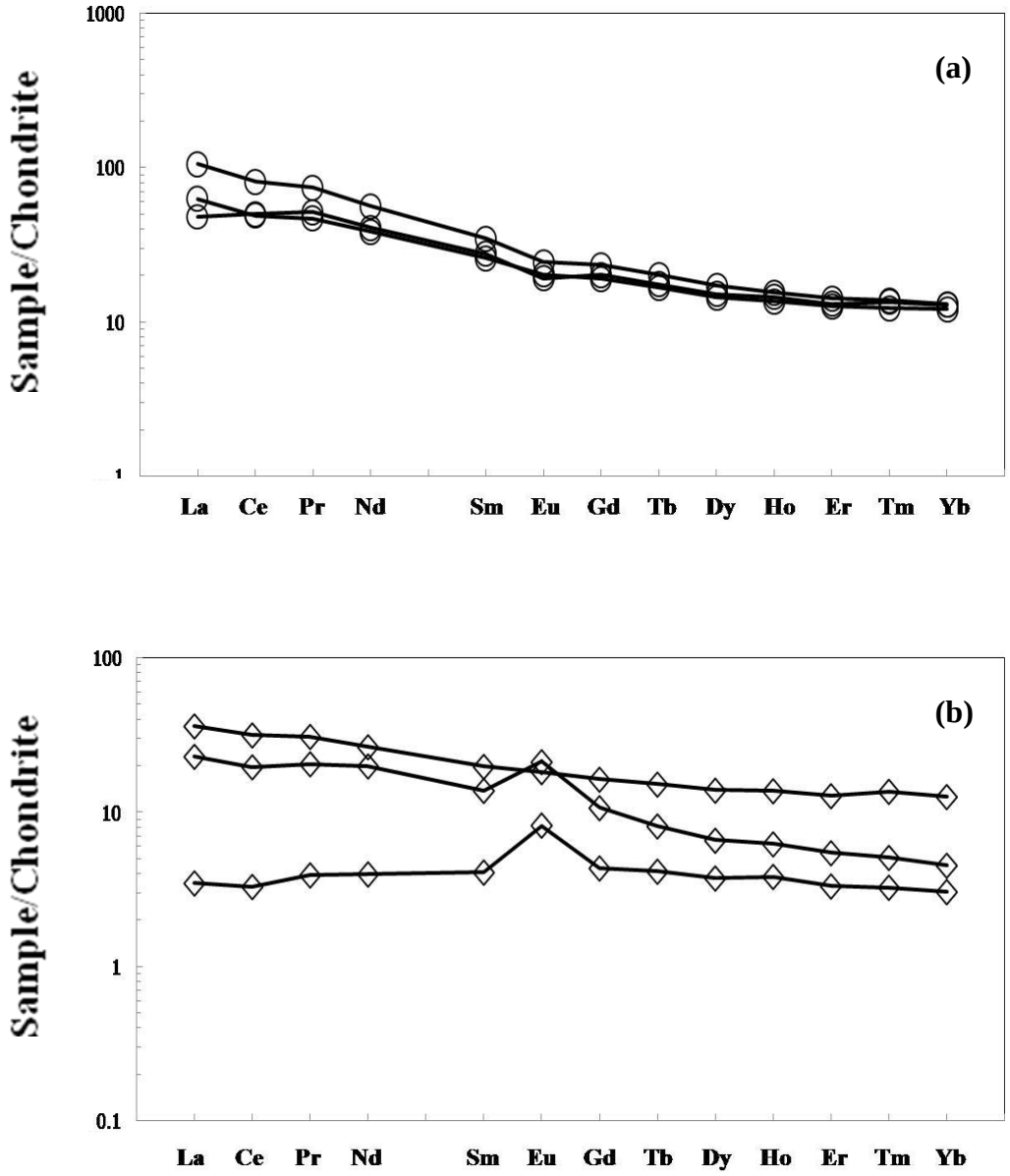

Figure 4.2 Chondrodite-normalized patterns for the representatives of (a) Group I and (b) Group II mafic igneous rocks. Chondrite-normalized values are those of Taylor and Gorton (1977).

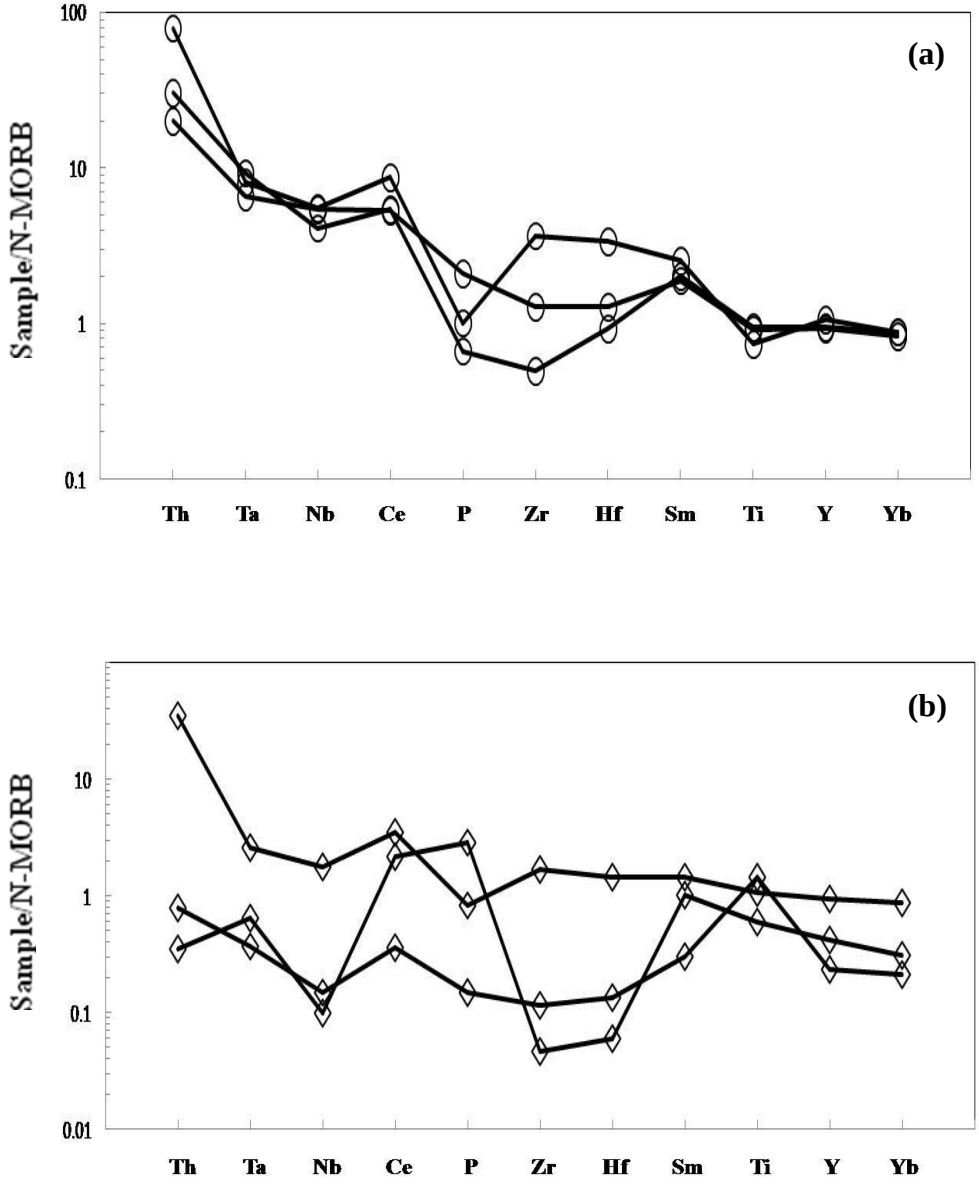

Figure 4.3 N-MORB normalized multi-element patterns for the representatives of (a) Group I and (b) Group II mafic igneous rocks. N-MORM normalized values are those of Sun and McDonough (1989).

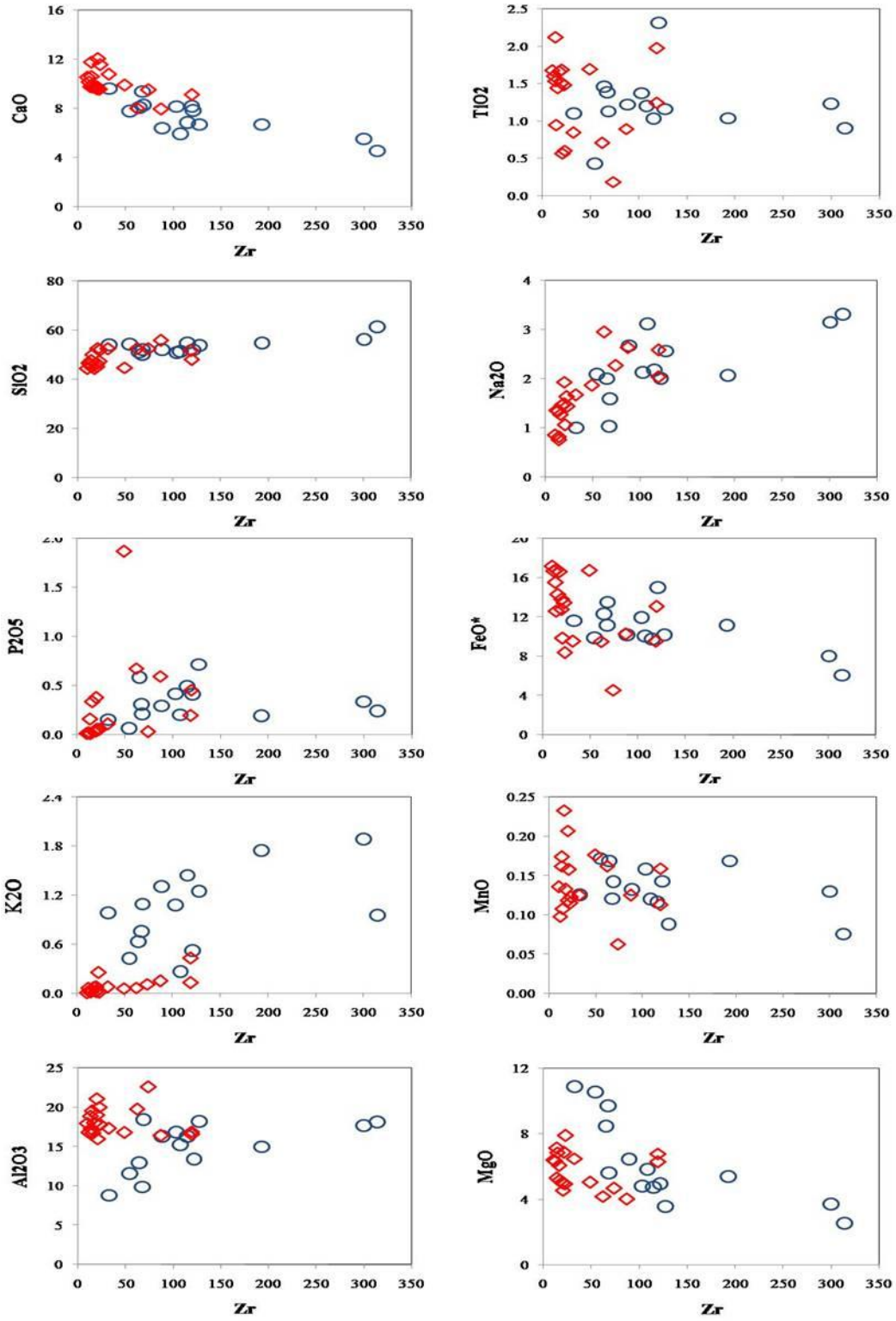

Figure 4.4 Zirconia variation diagrams for CaO, TiO_2, SiO_2, Na_2O, P_2O_5, FeO*, K_2O and MgO for the studied, least-altered mafic igneous rocks (open circle = Group I and open diamond=Group II). Zr is expressed as ppm, whereas major oxides as wt%.

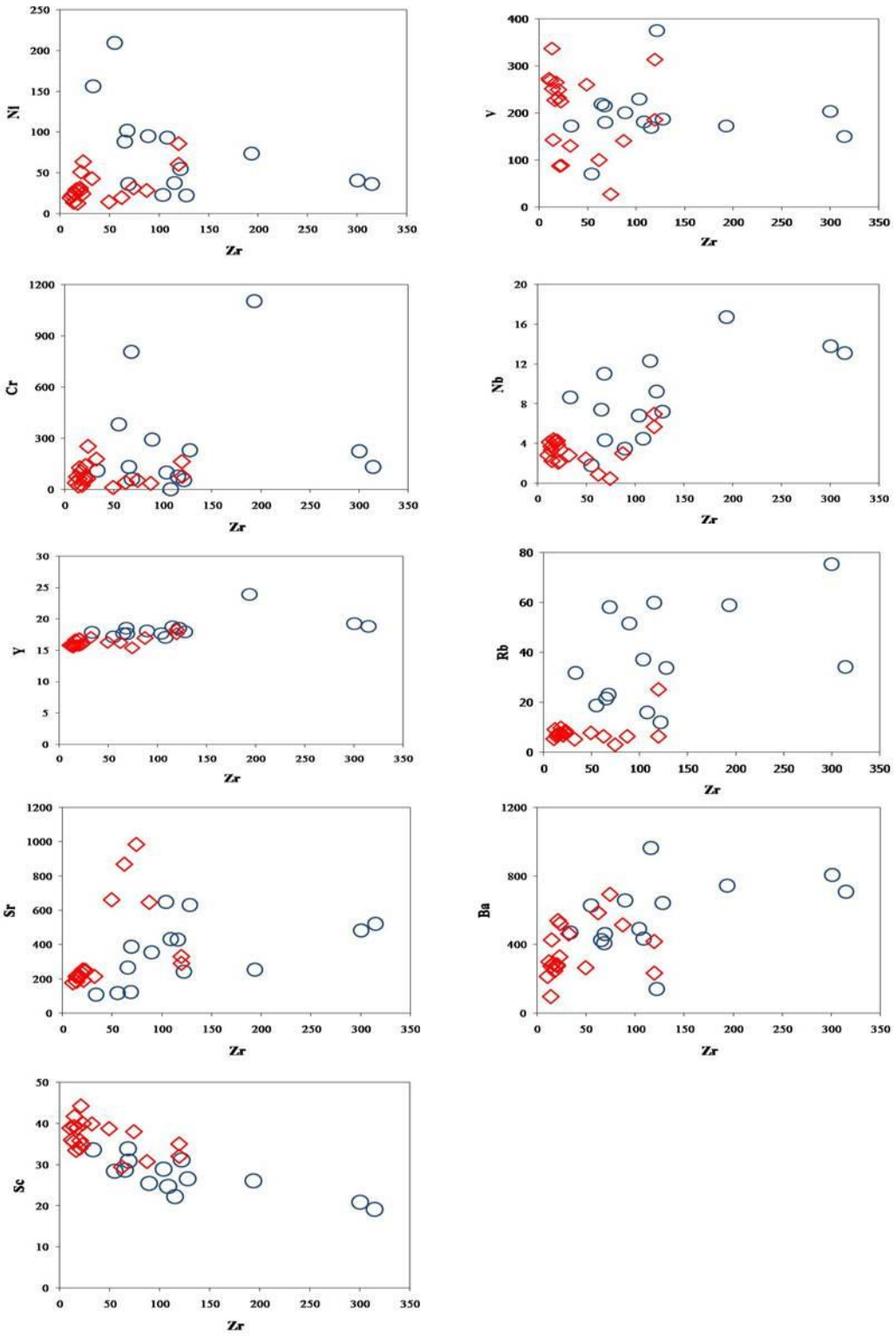

Figure 4.5 Zirconia variation diagrams for Ni, V, Cr, Nb, Y, Rb, Sr, Ba and Sr for the studied, least-altered mafic igneous rcoks (open circle = Group I and open diamond = Group II). All the trace elements are in ppm.

Group II, the diagrams show positive trends for SiO_2, Na_2O, P_2O_5, K_2O, Nb, Sr, Y, Rb and Ba and negative trends for CaO, MgO, FeO*, Al_2O_3, MnO, Ni, Cr, and Sc. The Ti and V are not shown trends in diagrams. The trends indicate that spinel and mafic minerals, such as olivine, pyroxene and/or amphibole.

The binary ratios and patterns of plotting in variation diagrams for two groups supported that they are not comagmatic.

4.5 Tectonic Setting of Eruption

4.5.1 Tectonic Discrimination Diagrams

Discrimination diagrams (Rollison, 1993) is geochemical variation diagrams on which magmas produced in different tectonic settings may be distinguished from one another on the basis of their chemistry. The elemental concentrations were calculated discrimination functions based upon the elemental concentrations, boundaries are drawn between the different groups of samples. The diagrams used to discriminate tectonic environments of the studied mafic rocks include Ti/Y-Nb/Y (Fig 4.6), V-Ti (Fig 4.7), Zr/Y-Ti/Y (Fig 4.8), Zr/Y-Zr (Fig 4.9), Cr-Y (Fig 4.10), Nb/Y-Zr/P_2O_5 (Fig 4.11), Ti-Zr (Fig 4.12) and TiO_2-Y/Nb (Fig 4.13) bivariate plots and Zr-Nb-Y (Fig 4.14), Zr-Ti-Y (Fig 4.15), Th-Hf-Ta (Fig 4.16) and La-Y-Nb (Fig 4.17) ternary plots.

The Group I rocks are present in the fields of largely of within-plate basalt, mid-oceanic ridge basalt and volcanic arc, with subordinate back-arc basin basalt, plate margin, continental tholeiitic basalt, ocean tholeittic basalt and calc-alkalic basalt. The within-plate basalt are present in Ti/Y-Nb/Y (Fig 4.6), Zr/Y-Ti/Y (Fig 4.8), Ti-Zr (Fig 4.12), Zr-Nb-Y (Fig 4.14) and Zr-Ti-Y (Fig 4.15) diagrams. The mid-oceanic ridge basalts are in Ti/Y-Nb/Y (Fig 4.6), V-Ti (Fig 4.7), Ti-Zr (Fig 4.12), Zr-Nb-Y (Fig 4.14) and Zr-Ti-Y (Fig 4.15) diagram. The field of volcanic arc is in Cr-Y (Fig 4.10), Zr/Y-Zr (Fig 4.9), Ti-Zr (Fig 4.12), Zr-Nb-Y (Fig 4.14) and Zr-Ti-Y (Fig 4.15) diagrams. The back-arc basin basalt is found in V-Ti (Fig 4.7) diagram. The plate margin plot in Zr/Y-Ti/Y (Fig 4.8) diagram. The field of continental tholeiitic

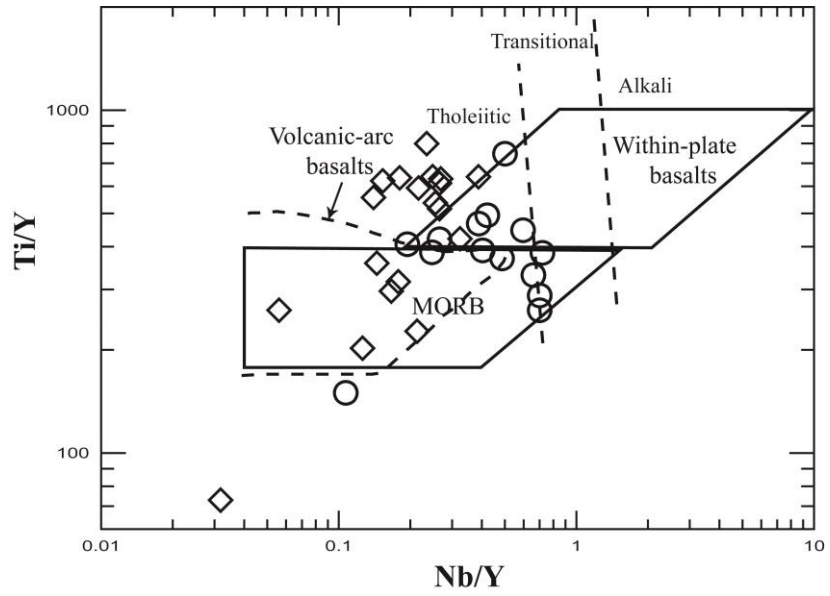

Figure 4.6 Ti/Y-Nb/Y discrimination diagram (after Pearce, 1982) for the studied, least-altered mafic igneous rocks (open circle = Group I and open diamond = Group II). MORB = mid-oceanic ridge basalt.

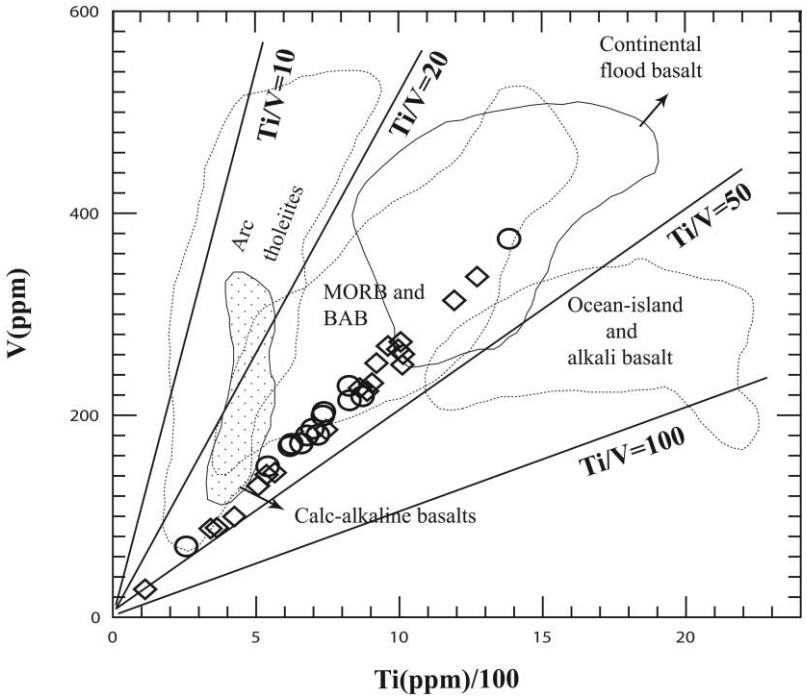

Figure 4.7 Ti-V tectonic discrimination diagram (after Shervais, 1982) for the studied, least-altered mafic igneous rocks (open circle = Group I and open diamond = Group II). The number given along the solid straight lines are Ti/V ratios.

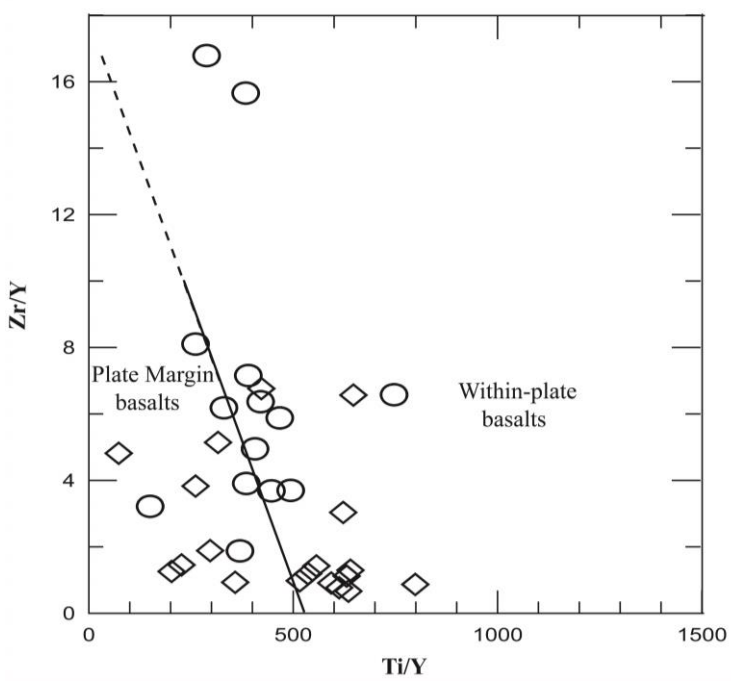

Figure 4.8 Zr/Y-Ti/Y discrimination diagram between plate-margin basalt and within-plate basalt (after Pearce and Gale, 1977) for the studied, least-altered mafic igneous rocks (open circle = Group I and open diamond = Group II).

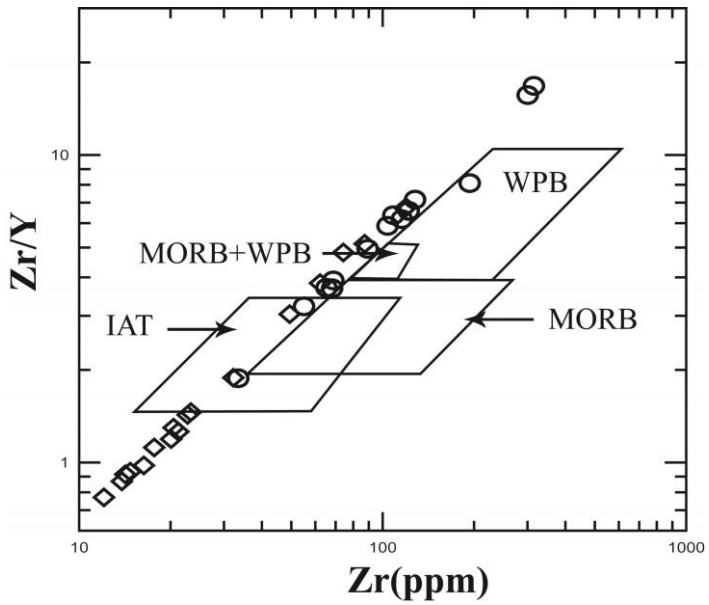

Figure 4.9 Zr/Y-Zr discrimination diagram (after Pearce and Norry, 1979) for the studied, least-altered mafic igneous rocks (open circle = Group I and open diamond = Group II). The fields are as follow: IAT = island-arc tholeiite, MORB = mid-oceanic ridge basalt, WPB = within-plate basalt.

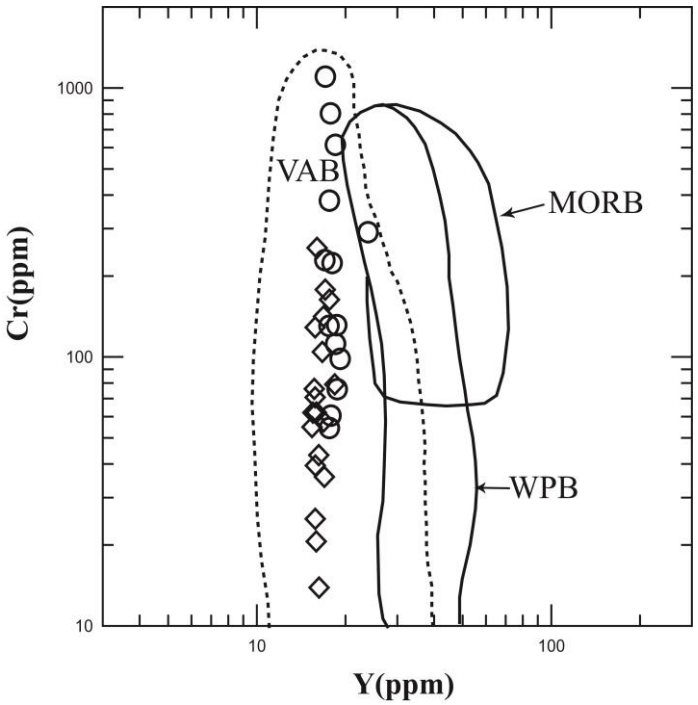

Figure 4.10 Cr-Y discrimination diagram (after Pearce, 1982) for the studied, least-altered mafic igneous rocks (open circle = Group I and open diamond = Group II). The fields are as follow: VAB = volcanic-arc basalt, MORB = mid-oceanic ridge basalt, WPB = within-plate basalt.

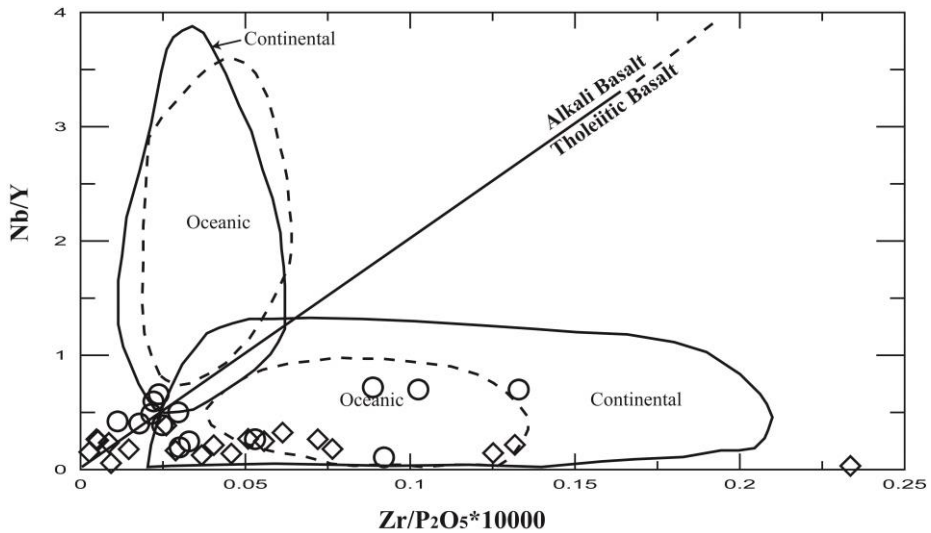

Figure 4.11 Nb/Y-Zr/P_2O_5 discrimination diagram (adapted from Floyd and Winchester, 1975) for the studied, least-altered mafic igneous rocks (open circle = Group I and open diamond = Group II). Showing fields of continental and oceanic alkali basalts and tholeiitic basalts.

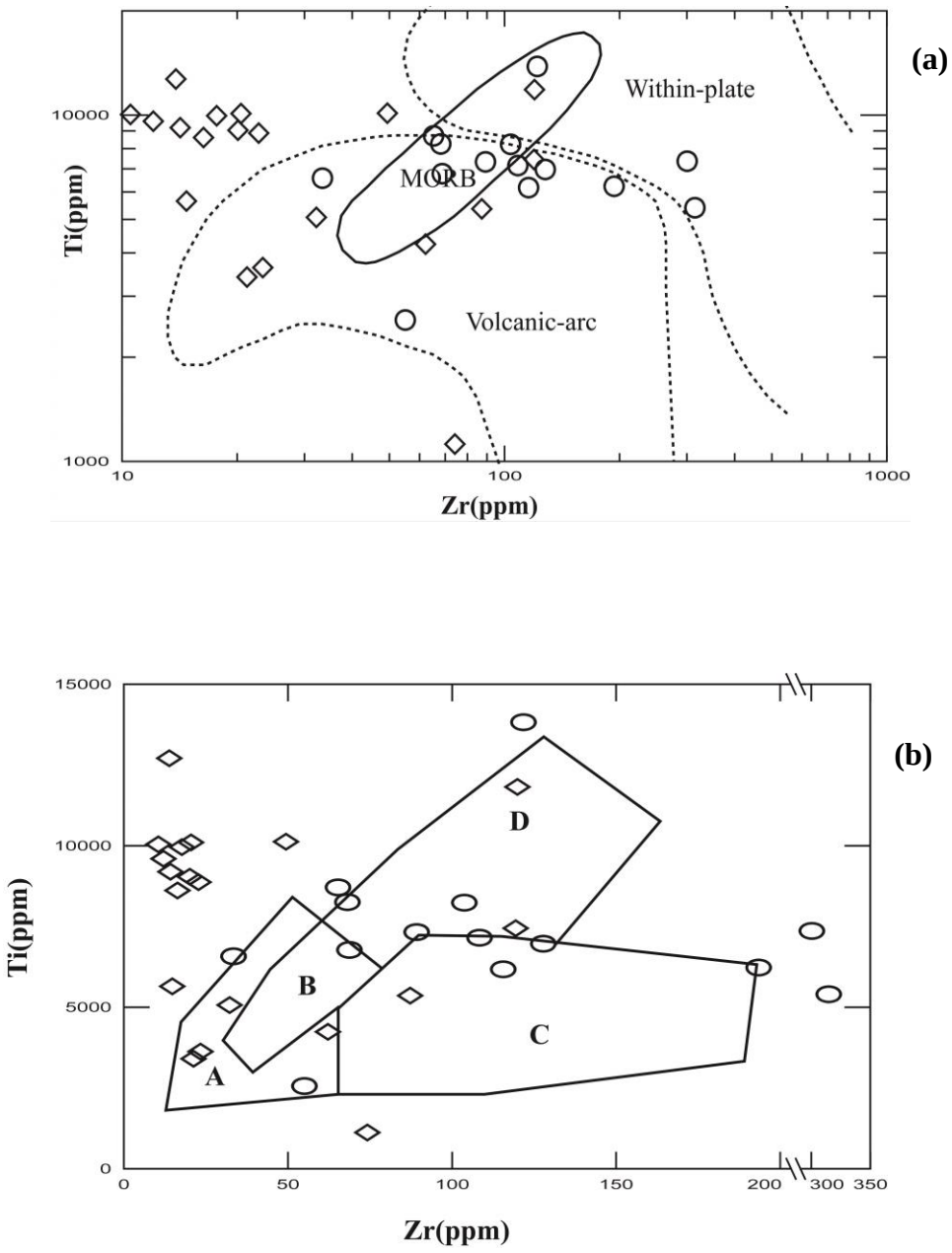

Figure 4.12 Ti-Zr discrimination diagram for the studied, least-altered mafic igneous rocks (open circle = Group I and open diamond = Group II), (a) after Pearce (1982) and (b) after Pearce and Cann (1973); the fields are as follows: MORB = mid-oceanic ridge basalt, A = island-arc tholeiites, B = mid-oceanic ridge basalt, calc-alkali basalts and island-arc tholeiites, C = calc-alkali basalts and D = mid-oceanic ridge basalt.

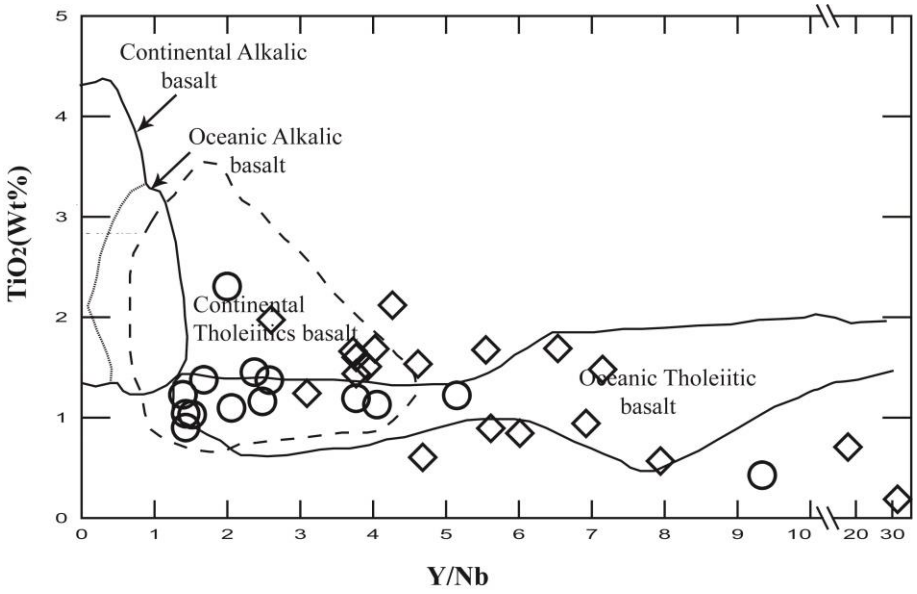

Figure 4.13 TiO_2-Y/Nb discrimination diagram (from Floyd and Winchester, 1975) for the studied, least-altered mafic igneous rocks (open circle = Group I and open diamond = Group II).

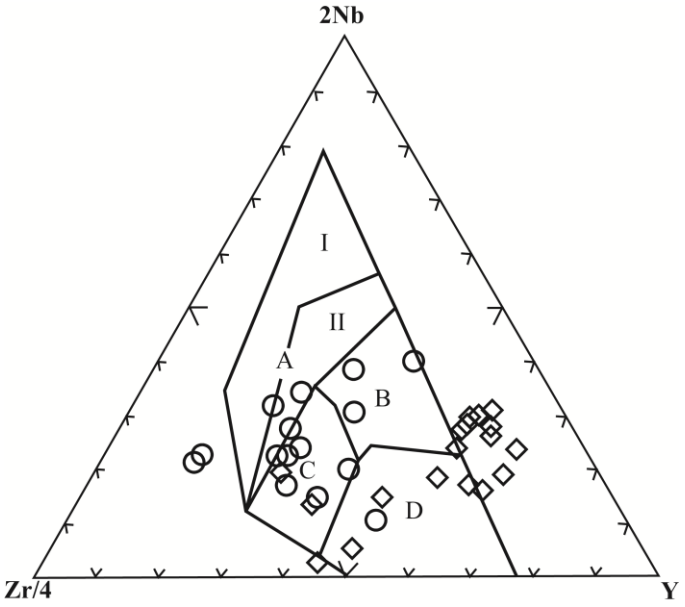

Figure 4.14 The Zr-Nb-Y discrimination diagram for the studied, least-altered mafic igneous rocks (open circle = Group I and open diamond = Group II) (after Meschede, 1986). The fields are defined as follows; AI = within-plate alkali basalts, AII = within-plate alkali basalts and within-plate tholeiites, B = enriched-mid oceanic ridge basalts, C = within-plate tholeiites and volcanic-arc basalts and D = normal-mid oceanic ridge basalts and volcanic-arc basalts.

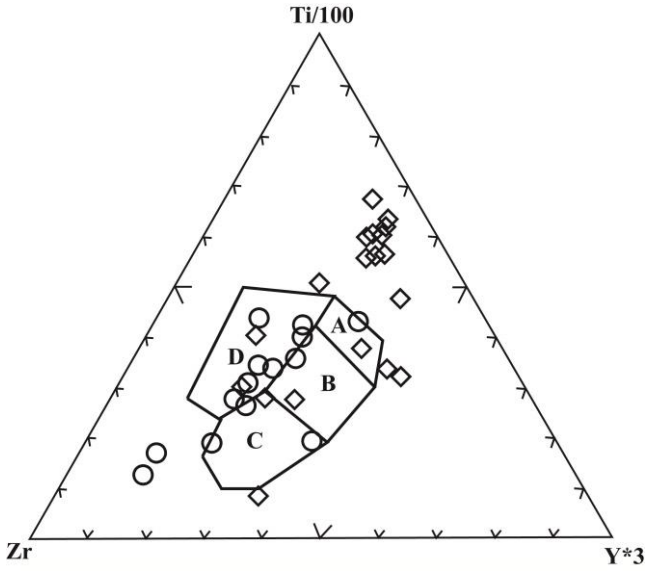

Figure 4.15 The Zr-Ti-Y discrimination diagram for the studied, least-altered mafic igneous rocks (open circle=Group I and open diamond=Group II). (after Pearce and Cann, 1973). The fields are as follows: A=island-arc tholeiite, C=calc-alkali basalt, D=within-plate basalt and B=MORB, island-arc tholeiite and calc-alkali basalt.

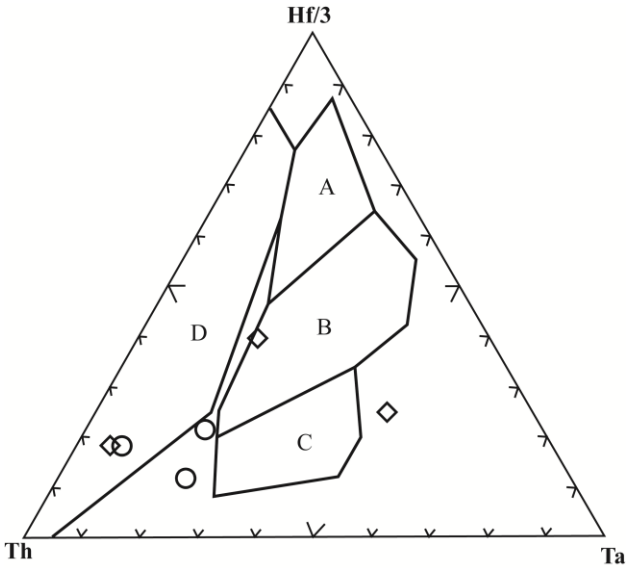

Figure 4.16 The Th-Hf-Ta discrimination diagram (after Wood, 1980) for the studied, least-altered mafic igneous rocks (open circle = Group I and open diamond = Group II). The fields are: A= normal mid-oceanic ridge basalts, B = enriched-mid oceanic ridge basalts and within-plate tholeiite, C=within-plate alkali basalt and D = volcanic-arc basalt. Island-arc tholeiite is in the field D where Hf/Th>3.0 and calc-alkalic basalt where Hf/Th<3.0.

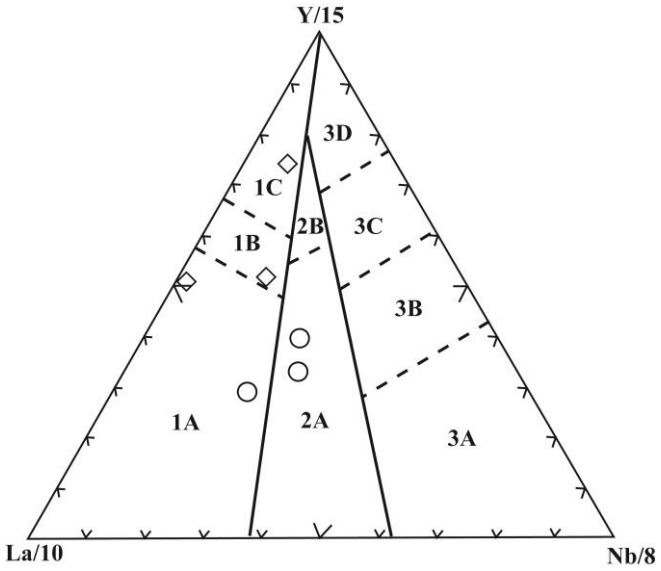

Figure 4.17 The La-Y-Nb discrimination diagram (after Cabanis and Lecolle, 1989) for the studied, least-altered mafic igneous rocks (open circle = Group I and open diamond = Group II). Field1 contains volcanic-arc basalt, field2 continental basalt, and field3 oceanic basalt. The subdivisions of the fields are as follows: 1A = calc-alkali basalt, 1C = volcanic-arc tholeiite, 1B = calc-alkali basalt and volcanic are tholeiite, 2A = continental basalt, 2B = back-arc basin, 3A = alkali basalt from intercontinental rift, 3B+3C = enriched-mid oceanic ridge basalts (3B enriched, 3C weakly enriched), and 3D = normal-mid oceanic ridge basalts.

basalt is in Nb/Y-Zr/P_2O_5 (Fig 4.11), TiO_2-Y/Nb (Fig 4.13), Th-Hf-Ta (Fig 4.16) and La-Y-Nb (Fig 4.17) diagrams. The oceanic tholeiitic basalt and calc-alkalic basalt are present in Th-Hf-Ta (Fig 4.16) and La-Y-Nb (Fig 4.17) diagrams.

The Group II rocks emerge to be the fields of largely of mid-oceanic ridge basalt and volcanic arc, with subordinate plate margin, within-plate, back-arc basin basalt, continental tholeiitic basalt, ocean tholeittic basalt and calc-alkalic basalt. The mid-oceanic ridge basalt is present in Ti/Y-Nb/Y (Fig 4.6), V-Ti (Fig 4.7), Zr-Nb-Y (Fig 4.14) and Zr-Ti-Y (Fig 4.15) diagram. The volcanic arc is located in Ti/Y-Nb/Y (Fig 4.6), Cr-Y (Fig 4.10), Zr/Y-Zr (Fig 4.9), Ti-Zr (Fig 4.12), Zr-Ti-Y (Fig 4.15) and La-Y-Nb (Fig 4.17) diagrams. The plate margin and within-plate are in Zr/Y-Ti/Y (Fig 4.8) diagram. The back-arc basin basalt is present in V-Ti (Fig 4.7) and Zr-Nb-Y (Fig 4.14) diagrams. The continental and oceanic tholeiitic basalt is in Nb/Y-Zr/P_2O_5 (Fig 4.11) and TiO_2-Y/Nb (Fig 4.13) diagrams. The calc-alkalic basalt is present in Th-Hf-Ta (Fig 4.16) diagram.

4.5.2 Modern Analogue

Extensive searchers for modern analogue have been made in terms of chondrite-normalized REE and N-MORB normalized multi-element patterns. The modern analogues have been carried out to classify the tectonic settings of formation and for particular magmatic groups are given below.

The Group I rocks are closely similar in chemical composition to tholeiitic basalt (sample number 14-100 Alexa) from western Samoa Seamount (submarine volcano) (Fig 4.18) (Hart *et al.*, 2004). The Samoa ocean island basalts form as a hotspot chain in southwest Pacific plate, north of Tonga Trench.

The representative of the Group II rocks are chemically comparable with the immature back arc basin basalts (Fig 4.19) from the latest Jurassic greenstone belt in Hokkaido, northernmost island of Japan, constitutes the ultramafic-mafic units of SoShubetu-Chiroro area, Horokanai ophiolite (Takashima *et al.*, 2002). This Zone consists of aphyric tholeiite resembling back arc basin (BABB) tholeiite along with high –Mg andesite (sample number SS08).

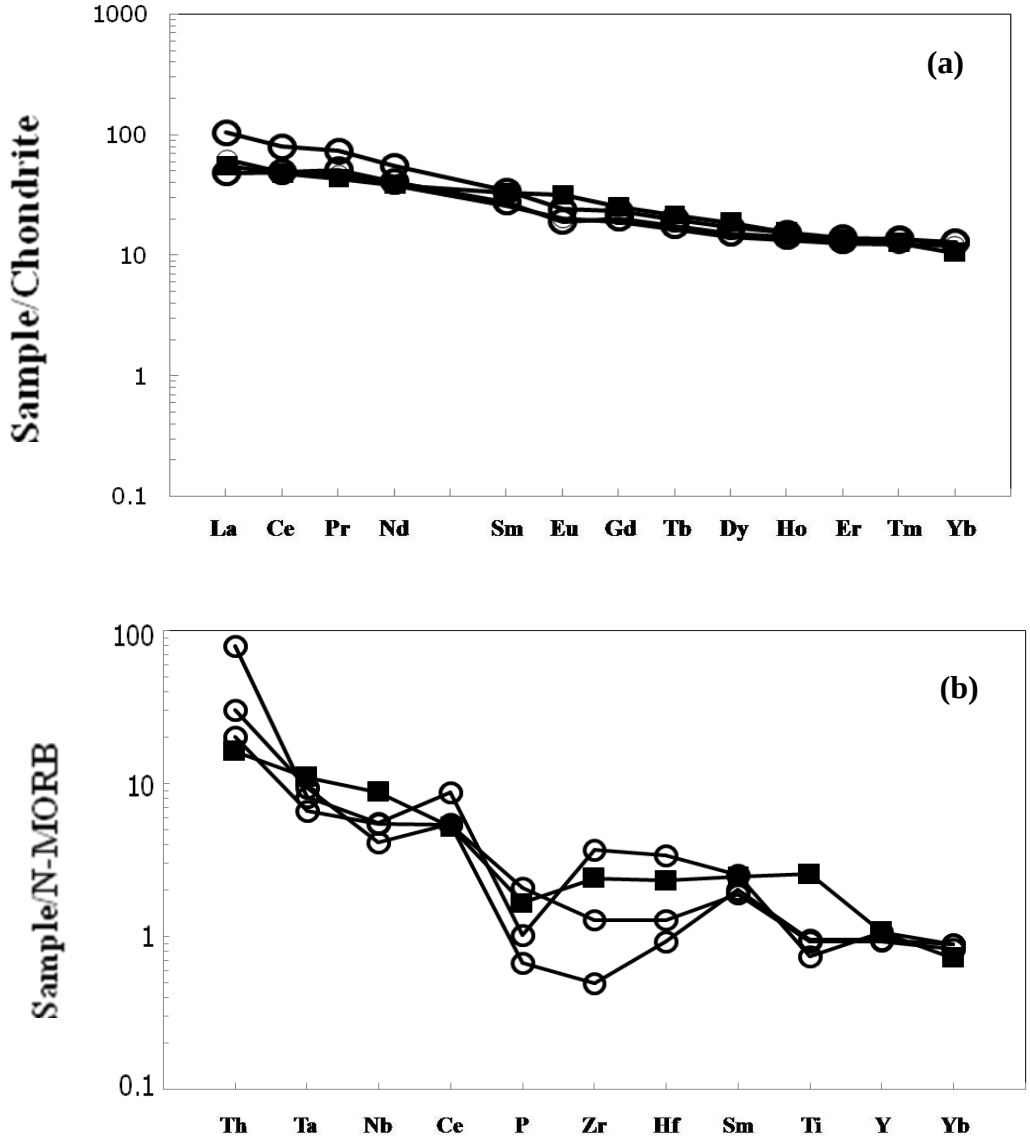

Figure 4.18 Chondrite-normalized REE patterns (a) and N-MORB normalized multi-element patterns (b) for the studied, least-altered mafic igneous rocks of Group I (open circle) and their modern analogue; tholeiitic basalt (sample number 14-100 Alexa, solid square) from western Samoa Seamont, southwest Pacific plate (Hart *et al.*, 2004). Chondrite-normalized values are those of Taylor and Gorton (1977) and N-MORB normalized values are those of Sun and McDonough (1989).

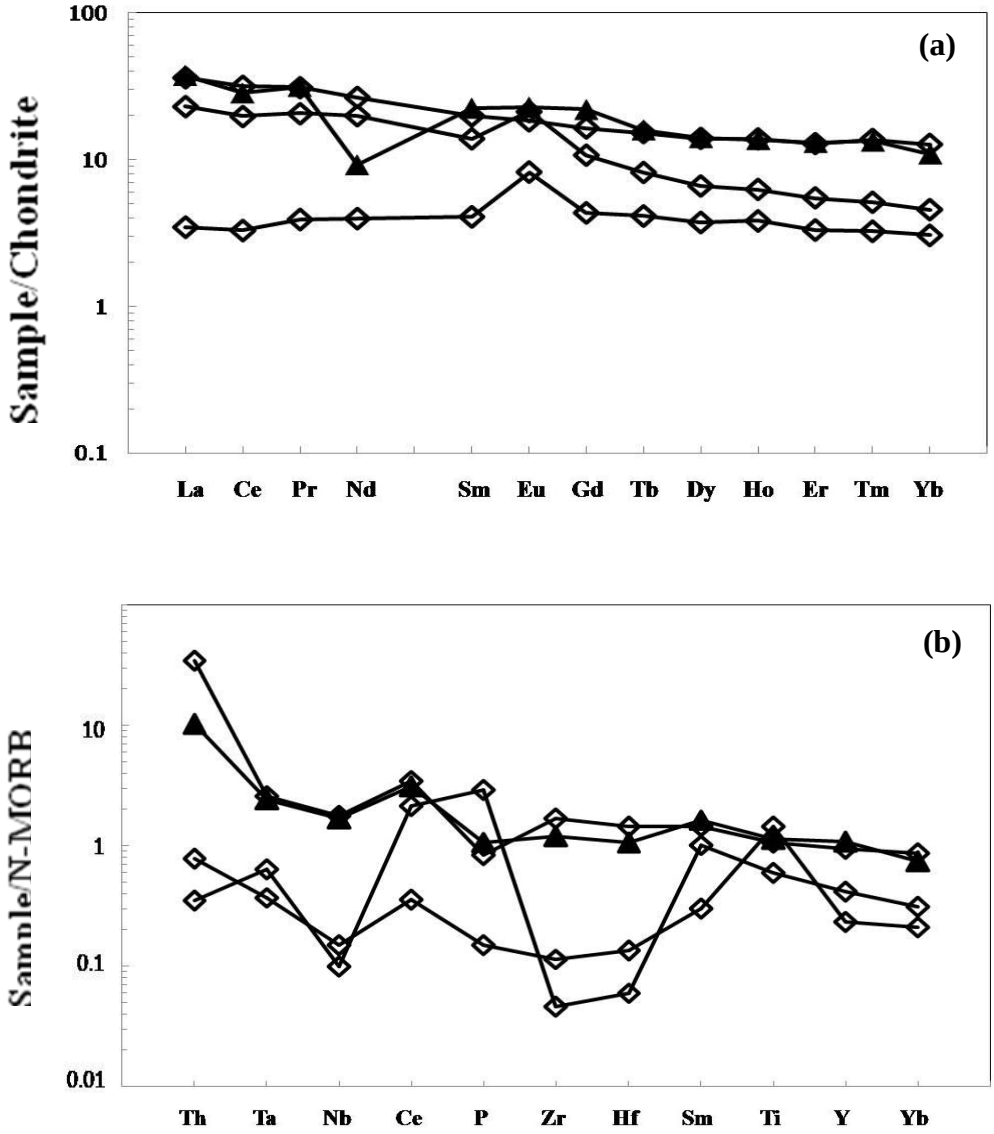

Figure 4.19 Chondrite-normalized REE patterns (a) and N-MORB normalized multi-element patterns (b) for the studied, least-altered mafic igneous rocks of Group II (open diamond) and their modern analogue; immature back arc basin basalts from Hokkaido (sample number SS08, solid triangle), Japan (Takashima *et al.*, 2002). Chondrite-normalized values are those of Taylor and Gorton (1977) and N-MORB normalized values are those of Sun and McDonough (1989).

4.5.3 Summary

It is obvious that the data of the tectonic discrimination diagrams may distribute scatteringly and may yield inconsistent results. These diagrams may fail to clearly classify tectonic setting of formation. Therefore, the problem can be solved by extensive search for the modern analogues of the least-altered mafic igneous rocks, particularly in terms of chondrite-normalized and N-MORB normalized multi-immobile element patterns.

In Modern analogues, the concentrations of immobile incompatible elements and REE of the Group I rocks are closely similar in chemical composition to tholeiitic basalt from the Samoa ocean island basalts form as a hotspot chain in southwest Pacific plate, north of Tonga Trench. The concentrations of immobile incompatible elements and REE of the Group I rocks of the Group II rocks are chemically comparable with the immature back arc basin basalts from the latest Jurassic greenstone belt in Hokkaido, northernmost island of Japan.